Parsimonious Channel Models for Millimeter Wave Railway Communications

Erich Zöchmann*†‡, Jiri Blumenstein‡, Roman Marsalek‡, Markus Rupp†, and Ke Guan§
*Christian Doppler Laboratory for Dependable Wireless Connectivity for the Society in Motion
†Institute of Telecommunications, TU Wien, Austria
‡Department of Radio Electronics, Brno University of Technology, Czech Republic
§State Key Laboratory of Rail Traffic Control and Safety, Beijing Jiaotong University, China

***Abstract*—We show that the deterministic two-ray model and the statistical two-wave with diffuse power (TWDP) model are suitable channel models for millimeter wave train-to-infrastructure wireless communications. Both models make parsimonious use of model parameters and are therefore implementable with very low complexity. Once directive antennas are employed, such models turn out to be accurate. The wireless channel is mainly dominated by the line-of-sight component and a ground reflection then. These two components lead to an oscillatory interference pattern with instantaneous frequency defined by the geometry. We derive fading envelopes to find a simple parametrization of the TWDP model through the deterministic two-ray model. The effectiveness of our approach is demonstrated on ray-tracing data.**

***Index Terms*—Directive Antennas, Fading, Millimeter Wave, Parameter Extraction, Railway Communications, TWDP, Two-Ray Model, V2X Communications**

I. Introduction

Interestingly, millimeter wave (mmWave) frequency bands have been candidates for vehicular communications already for several decades [1]–[3]. The key to a better understanding of (mmWave) railway communications lies in reasonable channel modeling [4], [5].

At lower frequencies measurements have been made to predict the performance for railway communications [6]–[10]. However, for mmWaves, accurate, yet simple channel models, inevitable for link-level performance studies [11]–[14], are still lacking.

In our prior work [15], based on ray-tracing data, we already demonstrated that railway communication scenarios employing directive antennas are effectively modeled via a two-ray model. Traditionally, the multi-slope behavior of the observed path loss was explained by a two-ray (ground reflection) model [16], [17]. The applicability of the two-ray model for the current dedicated short range communication (DSRC) standard around $5.9\,\mathrm{GHz}$ is shown in [18]–[20]. Especially for millimeter waves, it has been observed that channels are dominated by a few multipath components [21]–[30], and therefore, models employing only a few rays are even better justified. Evidence for the two-ray model can also be found in [31], where the deviations from the two-ray model were explained by road undulations. These road undulations, or in the train context the heterogeneous ground and the hardly predictable reflection coefficient, motivate us to transform the deterministic two-ray model into the statistical Two-Wave with Diffuse Power (TWDP) model.

Our Contributions

We demonstrate on ray-tracing data [32] that the two-ray model is a suitable deterministic small-scale fading model for line-of-sight (LOS) mmWave scenarios. We derive fading envelopes depending on antenna alignments, geometry, and bandwidth.

Next, we argue that the two-ray model is a specific, deterministic variant of the statistical TWDP model. For enclosed structures, such as aircraft cabins and buses, the applicability of the TWDP model is demonstrated by Frolik [33]–[35]. The TWDP model is flexible enough to accommodate additionally smaller multipath components as so called diffuse components. Furthermore through statistical modeling, uncertainties, for example, about reflection phases, road undulations, or path lengths, are automatically included. The derived quantities of the two-ray model will serve to parametrize the TWDP model.

II. Two-Ray Model

The two-ray (ground reflection) model has its widespread use as model for the path loss coefficient in wireless communications systems. Nevertheless, the two-ray model is a small-scale fading model as it describes an interference pattern of two waves. Analogously to [36], the description in the delay domain supports our arguments. Our analyzed scenario, leading to a two-ray model, is depicted in Fig. 1.

A. Time-Domain Description

The channel impulse response of the two-ray model reads

$$h(d,\tau) = a(d)\big(\delta(\tau) + g(d)\mathrm{e}^{\mathrm{j}\phi(d)}\delta(\tau-\tau_0(d))\big)\ , \qquad (1)$$

where a subsumes the free space attenuation of the LOS path of length l_L and the distance-dependent antenna gains of the transmitter $G_\mathrm{L}^\mathrm{TX}(d)$ and receiver $G_\mathrm{L}^\mathrm{RX}(d)$, respectively. By the notation $G_\mathrm{L}^\mathrm{TX}(d)$ we stress that the antenna gains for a given geometry and beamforming strategy (fixed beamforming or dynamic beamforming) are only dependent on the distance

The financial support by the Austrian Federal Ministry for Digital and Economic Affairs and the National Foundation for Research, Technology and Development is gratefully acknowledged. The research described in this paper was co-financed by the Czech Science Foundation, Project No. 17-18675S Future transceiver techniques for the society in motion.

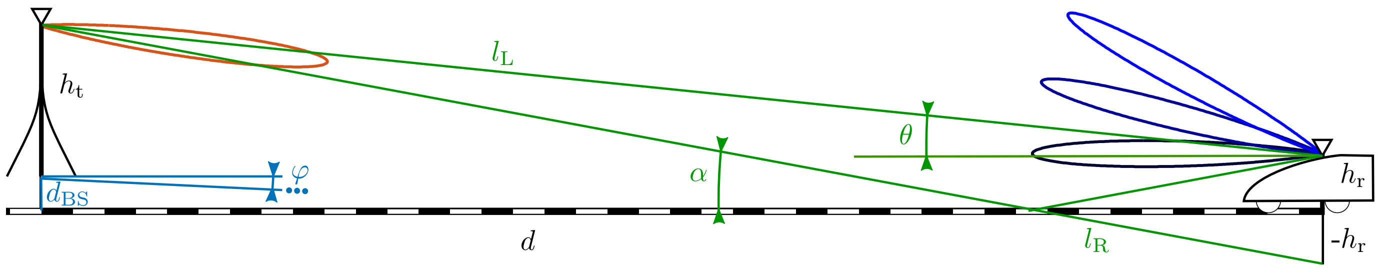

Fig. 1. A sketch of the analyzed scenario. We study train-to-infrastructure communications where the base station is employing a directive antenna with static alignment and only the approaching train adapts the beam direction in elevation θ and azimuth φ. The base station is $d_{\mathrm{BS}} = 10\,\mathrm{m}$ away from the train tracks. The base station is pointing its beam to the tracks at $d = 500\,\mathrm{m}$. Throughout the paper we will approximate $l_{\mathrm{L}} \approx l_{\mathrm{R}} \approx d$. The base station height is $h_t = 10\,\mathrm{m}$ and the antenna on the train is mounted on a height of $h_r = 3\,\mathrm{m}$. The antennas have 25 dBi gain. More details are found in [32].

d. In other words, given the alignments and the height of the antennas, the elevation and the azimuth angle of the transmitted and received waves are implicitly given. Subscript L or R reflects whether we focus on the LOS component or on the reflected one. For distances $d \gg h_{\mathrm{t}}, h_{\mathrm{r}}$ much longer than the transmitter and receiver height, the factor a is commonly approximated to

$$a(d) \approx \frac{\lambda\sqrt{G_{\mathrm{L}}^{\mathrm{TX}}(d)G_{\mathrm{L}}^{\mathrm{RX}}(d)}}{4\pi d} \ . \tag{2}$$

Despite the large bandwidths of mmWave systems, the relative bandwidth is mostly below 5% which allows us to drop the frequency dependency of a through fixing the wavelength λ to the center frequency. The second, reflected and delayed component, has analogously a (complex) path attenuation of

$$a_{\mathrm{R}}(d) \approx \frac{\lambda\sqrt{G_{\mathrm{R}}^{\mathrm{TX}}(d)G_{\mathrm{R}}^{\mathrm{RX}}(d)}}{4\pi d}\mathrm{e}^{\mathrm{j}\phi(d)} \ , \tag{3}$$

where ϕ models the phase change due to reflection. We factor out the gain of the LOS component and describe the reflected component by the relative loss function

$$g(d) = \sqrt{\frac{G_{\mathrm{R}}^{\mathrm{TX}}(d)G_{\mathrm{R}}^{RX}(d)}{G_{\mathrm{L}}^{\mathrm{TX}}(d)G_{\mathrm{L}}^{\mathrm{RX}}(d)}} \ . \tag{4}$$

Assuming, again, a relatively long ground distance d we can approximate the delay of the reflected component to [15]

$$\tau_0(d) = \frac{\Delta l}{c} = \frac{2h_{\mathrm{t}}h_{\mathrm{r}}}{d}\frac{1}{c} \ . \tag{5}$$

If we employed a system bandwidth that resolves delay τ_0 in (1), we could collect the energy of both rays by a multipath receiver, for example, a rake receiver. The receive power $\|h(\tau)\|^2$ then falls off exponentially with distance. A narrowband receiver cannot resolve both rays and simply adds them up. Depending on the delay (phase) of both paths, an interference pattern is caused by the receive filter convolution.

B. Frequency-Domain Description

As mentioned above, depending on the bandwidth, we either are possible to resolve both paths and no fading will be present, or we do not have enough time resolution and fading will occur. To analyze the strength of the fading process we derive the mean power (*large-scale fading*) and envelope formulas for constructive interference and for destructive interference (*small-scale fading*) in the frequency domain. In the following derivations we drop the function arguments (braces) to achieve compact equations.

The Fourier transform of (1) reads

$$\mathcal{FT}\{h(d,\tau)\} = H(d,f) = a\left(1 + g\,\mathrm{e}^{-\mathrm{j}(2\pi\tau_0 - \phi)}\right) \tag{6}$$

The power spectral density is calculated as the magnitude square of the Fourier transform (6)

$$\begin{aligned}\left|H(d,f)\right|^2 &= a^2\left(1 + g^2 + 2g\cos\left(2\pi f\tau_0 - \phi\right)\right)\\ &= a^2\left(1 + g^2 + 2g\cos\left(\frac{4\pi}{\lambda}\frac{h_{\mathrm{t}}h_{\mathrm{r}}}{d} - \phi\right)\right) \ . \end{aligned}\tag{7}$$

To calculate the large-scale fading we average the power spectrum on a confined area. The functions a and g are changing relatively slowly with changing distance, but the term $\cos(\frac{4\pi}{\lambda}\frac{h_{\mathrm{t}}h_{\mathrm{r}}}{d} - \phi)$ in (7) has a spatial fading period [36] of

$$\Delta d|_{2\pi} = \frac{\lambda d^2}{2h_{\mathrm{t}}h_{\mathrm{r}}} = \frac{\lambda d}{\Delta l} \ . \tag{8}$$

Spatial averaging over a length of $\Delta d|_{2\pi}$ removes the small-scale fluctuations leaving only the large-scale fading

$$\overline{\left|H(d)\right|^2} = a(d)^2\left(1 + g(d)^2\right) \ . \tag{9}$$

Next we calculate the constructive and destructive envelope of the two-ray model. The effect of the bandwidth B is modeled through uniformly distributing the transmit power in $P_x \sim \mathcal{U}(f_0 - B/2, f_0 + B/2)$. The average receive power is then given by

$$\begin{aligned}\mathbb{E}_{P_x}\{|H|^2\} &= a^2(1+g^2) + 2a^2g\int_{f'=f_0-B/2}^{f_0+B/2}\frac{1}{B}\cos\left(2\pi f'\tau_0 - \phi\right)\mathrm{d}f'\\ &= a^2\left(1+g^2\right) + 2a^2g\cos(2\pi\tau_0 f_0 - \phi)\,\mathrm{sinc}(\tau_0 B) \ . \end{aligned}\tag{10}$$

The sinc function is defined as $\operatorname{sinc}(x) = \frac{\sin(\pi x)}{\pi x}$. As $-1 \leq \cos(2\pi\tau_0 f_0 - \phi) \leq 1$, the following receive power envelopes are achieved

$$\mathbb{E}_{P_x}\left\{|H|^2\right\} \leq a^2\left(1+g^2\right) + 2a^2 g\left|\operatorname{sinc}(\tau_0 B)\right| \tag{11a}$$
$$\mathbb{E}_{P_x}\left\{|H|^2\right\} \geq a^2\left(1+g^2\right) - 2a^2 g\left|\operatorname{sinc}(\tau_0 B)\right| . \tag{11b}$$

C. Simplistic Modeling of Directive Antennas

To calculate the envelopes given above, one needs to know the antenna pattern to compute Eq. (4). Sometimes, only the gain values or half-power beam width values at elevation $\theta_{3\mathrm{dB}}$ and azimuth $\varphi_{3\mathrm{dB}}$ of the directive antennas are the known variables. To keep the model applicable, a simplified antenna model is used at this point, in which the pattern is based on a cosine function taken to a higher power. By doing this, all values except for the extrema $-1, 1$ will progressively decrease. The exponent n is derived to fulfill the half-power beam width. For example, the exponent of the elevation pattern (E-plane) is chosen to ensure that

$$\cos\left(\frac{\theta_{3\mathrm{dB}}}{2}\right)^n \overset{!}{=} \frac{1}{2} \quad \Rightarrow \quad n = \frac{-1}{\operatorname{ld}\left(\cos\left(\frac{\theta_{3\mathrm{dB}}}{2}\right)\right)} , \tag{12}$$

where ld is the binary logarithm. The final gain pattern, including the mechanical alignments at elevation θ_{a} and azimuth φ_{a}, is given by

$$G(\theta, \theta_{\mathrm{a}}, \theta_{3\mathrm{dB}}, \varphi, \varphi_{\mathrm{a}}, \varphi_{3\mathrm{dB}}) = G_{\max} \tag{13}$$
$$\cos\left(\frac{\theta-\theta_{\mathrm{a}}}{2}\right)^{\frac{-1}{\operatorname{ld}\left(\cos\left(\frac{\theta_{3\mathrm{dB}}}{2}\right)\right)}} \cos\left(\frac{\varphi-\varphi_{\mathrm{a}}}{2}\right)^{\frac{-1}{\operatorname{ld}\left(\cos\left(\frac{\varphi_{3\mathrm{dB}}}{2}\right)\right)}} ,$$

The example patterns generated by Eq. (13) are illustrated in Fig. 2. To the best of the author's knowledge, this practical approach of obtaining equations for the antenna patterns has not yet been proposed, yet this approach is of course very related to the Gaussian beam model [37], [38]

$$G_{\text{Gauß}}(\theta, \theta_{\mathrm{a}}, \theta_{3\mathrm{dB}}, \varphi, \varphi_{\mathrm{a}}, \varphi_{3\mathrm{dB}}) = G_{\max} \tag{14}$$
$$\exp\left\{-4\ln(2)\left(\frac{\theta-\theta_{\mathrm{a}}}{\theta_{3\mathrm{dB}}}\right)^2\right\} \exp\left\{-4\ln(2)\left(\frac{\varphi-\varphi_{\mathrm{a}}}{\varphi_{3\mathrm{dB}}}\right)^2\right\} ,$$

where $\ln$ is the natural logarithm. However, there are drawbacks in using these methods: the missing side lobes and the inflexibility of the exact pattern since only half-power bandwidths are factored in.

Now the two-ray model, including the simplified antenna pattern in Eq. (13) and the derived Eq. (9) and Eq. (11), is compared with the ray-tracing data from [32] (see Fig. 3). In [32], the SNR data were studied. To obtain the SNR values from the proposed model, the transmit power is then set to $P_{\mathrm{T}} = 20\,\mathrm{dBm}$, and the noise figure is selected to be $N_{\mathrm{F}} = 10\,\mathrm{dB}$ (see [32]). The SNR is expressed as

$$\mathrm{SNR}\big|_{\mathrm{dB}} = P_{\mathrm{T}}\big|_{\mathrm{dBm}} + \mathbb{E}_{P_x}\left\{|H|^2\right\}\big|_{\mathrm{dB}} \tag{15}$$
$$- \left(-174\,\mathrm{dBm/Hz} + 10\log_{10}(B)\big|_{\mathrm{dBHz}} + N_{\mathrm{F}}\big|_{\mathrm{dB}}\right).$$

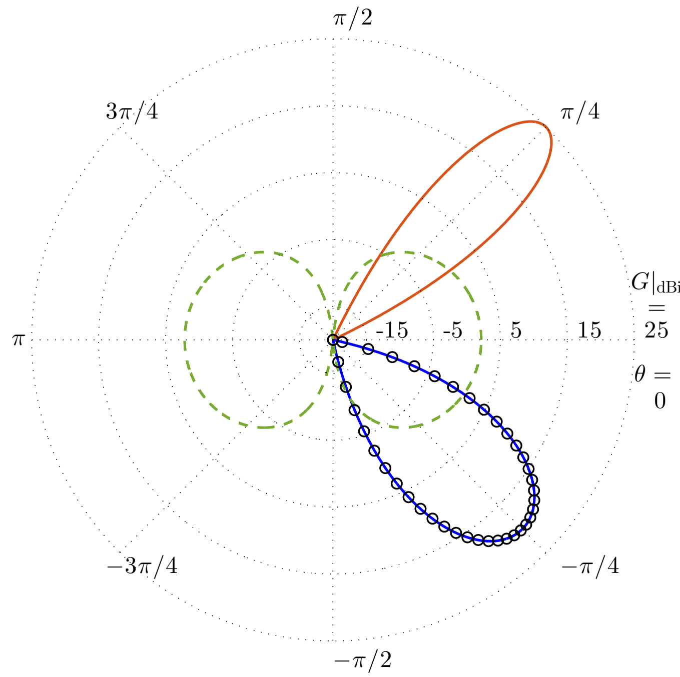

Fig. 2. The red directive pattern pointing toward $\pi/4$ is the antenna pattern used in this chapter ($\theta_{3\mathrm{dB}} = 10°$ and $G = 25\,\mathrm{dBi}$). The blue directive pattern pointing toward $-\pi/4$ is an example of a less directive antenna. The superimposed black circular markers are the result of the Gaussian beam model. The pattern of a $\lambda/2$ dipol is sketched in green dashed lines for comparison.

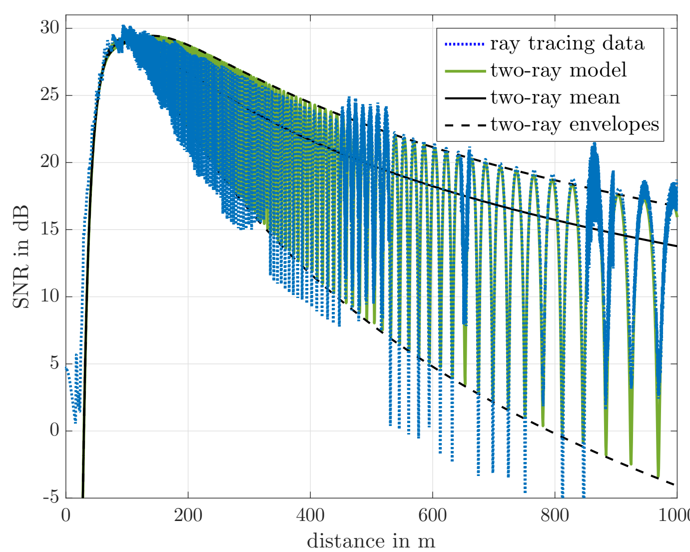

Fig. 3. The two-ray model allows for a good description of observed SNR in the ray-tracing study [32].

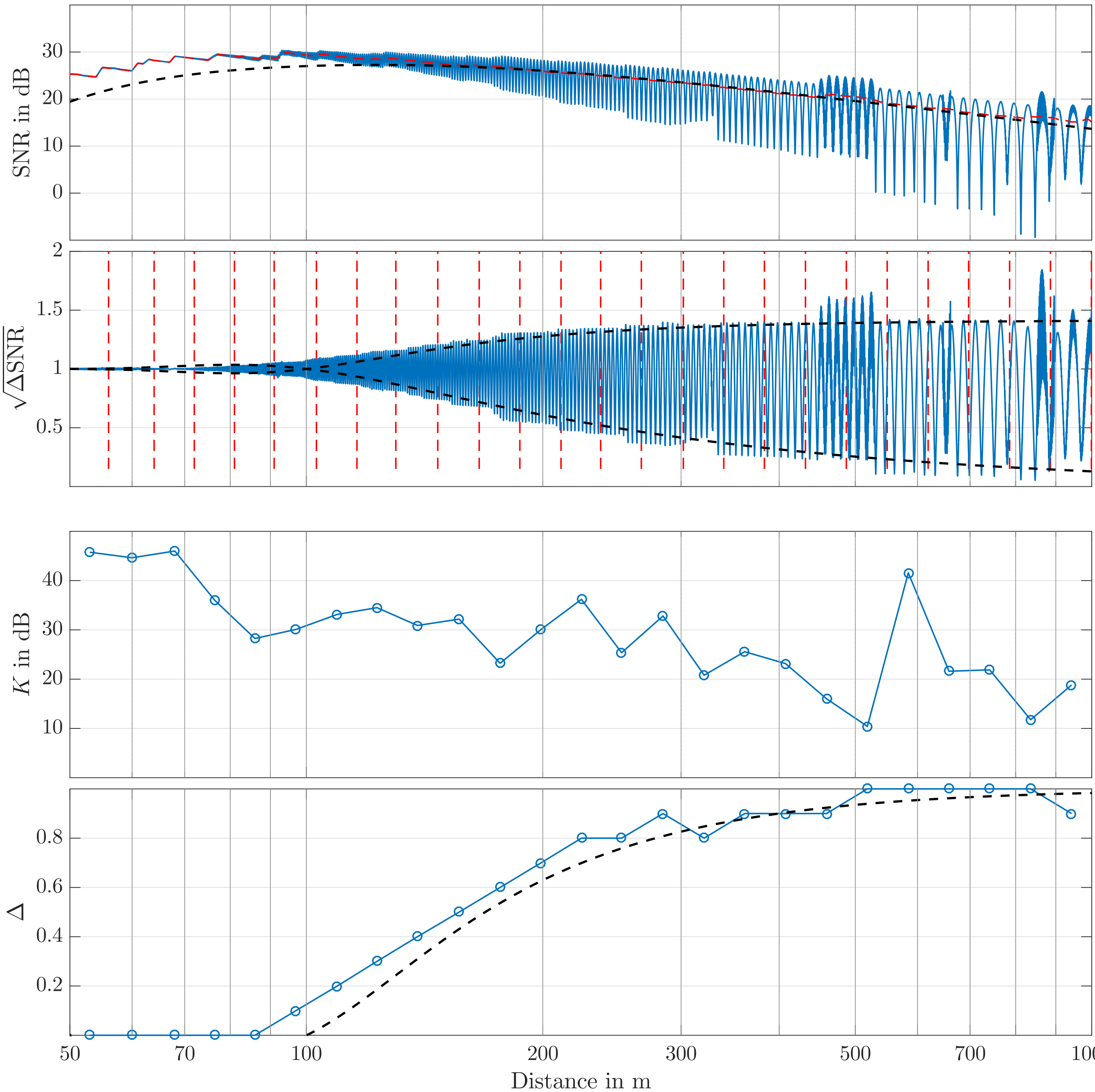

Fig. 4. Fitted large-scale fading, fading envelopes, and Δ-parameters. (Panel 1) The SNR from Fig. 3 is shown with logarithmic abscissa scaling. The black dashed line shows the predicted large-scale power from Eq. (9). The red dashed line shows the estimated large-scale power, which is computed through the sliding average approach. (Panel 2) The SNR fluctuations are shown by removing the large-scale trend. The envelopes given in Eq. (19) are plotted in black dashed lines. The red, dashed, vertical lines show the evaluation regions for the ML parameter estimation. (Panel 3) This shows the ML fitted K-parameter of the TWDP model. The K-factor decreases with increasing distance as the directive antenna illuminates more surrounding buildings; hence, more multipath components are generated. (Panel 4) This panel presents the ML fitted Δ-parameter of the TWDP model. The theoretical prediction generated from the proposed model is again plotted as a black dashed line. The prediction and observation agree well.

III. Two-Wave with Diffuse Power Model

The Two-Wave with Diffuse Power Fading (TWDP) small-scale fading model assumes fading due to the interference of two strong radio signals and numerous smaller, so called diffuse, signals. Although deterministic modeling as two-ray ground reflection model is possible, a statistical model captures uncertainties and variations, for example, about the phase change of the reflection.

A. Mathematical Model and Parameter Fitting

TWDP fading was first introduced in [39]. A more extensive mathematical description is provided in [40]. For the convenience of the reader, we briefly summarize [40]. The TWDP fading model in the complex-valued baseband is given as

$$r_{\text{complex}} = V_1 \mathrm{e}^{\mathrm{j}\phi_1} + V_2 \mathrm{e}^{\mathrm{j}\phi_2} + X + \mathrm{j}Y \ , \tag{16}$$

where $V_1 > 0$ and $V_2 \geq 0$ are the deterministic amplitudes of the non-fluctuating specular components. The phases ϕ_1 and ϕ_2 are independent and uniformly distributed in $[0, 2\pi)$. The diffuse components are modeled via the law of large numbers as $X + \mathrm{j}Y$, where $X, Y \sim \mathcal{N}(0, \sigma^2)$ are independent Gaussian random variables. If ϕ_1 and ϕ_2 are chosen deterministically and if $\sigma \to 0$, the TWDP model is turned again into the two-ray model. The K-factor is defined analogously to the Rician K-factor as the power ratio of the specular components and the diffuse components

$$K = \frac{V_1^2 + V_2^2}{2\sigma^2} \ . \tag{17}$$

The parameter Δ describes the amplitude relationship among the specular components

$$\Delta = \frac{2V_1V_2}{V_1^2 + V_2^2} \ . \tag{18}$$

The Δ-parameter is bounded between 0 and 1 and equals 1 iff both amplitudes are equal. A third parameter Ω captures the second moment (the average power) of the fading amplitude. As we use the TWDP model just for describing the small-scale fading (the fluctuations around the mean) we will force $\Omega \equiv 1$ through normalization.

To estimate the second moment $\hat{\Omega}$ of the ray-tracing data, we apply a sliding window estimate with adaptive window size. The window size is chosen to stretch over two spatial periods as defined in (8). The parameter tuple $(\hat{K}, \hat{\Delta})$ is estimated through the method of maximum likelihood (ML) estimation as in [30], [41].

B. Calculation of Δ based on the Envelopes

We normalize the envelopes (11) by the mean power (9) to achieve $\Omega \equiv 1$. The sum voltage V_Σ and difference voltage V_Δ of both waves is then given as

$$V_{\Sigma|\Delta} = \sqrt{1 \pm \frac{2g|\operatorname{sinc}(\tau_0 B)|}{1+g^2}} \ . \tag{19}$$

The following system of equations defines the individual voltages V_1, V_2

$$V_1 + V_2 = V_\Sigma \tag{20a}$$

$$V_1 - V_2 = V_\Delta \ . \tag{20b}$$

Through squaring (20a) and (20b) and adding them, the product of V_1 and V_2 derives to

$$V_1V_2 = \frac{g|\operatorname{sinc}(\tau_0 B)|}{1+g^2} \ . \tag{21}$$

Plugging (21) into the squared Eq. (20b), gives the condition

$$V_1^2 + V_2^2 = 1 \ . \tag{22}$$

Putting (21) and (22) into the definition of Δ leads to

$$\Delta(d) = \frac{2g|\operatorname{sinc}(\tau_0 B)|}{1+g^2} = \frac{2g(d)\left|\operatorname{sinc}\left(\frac{2h_t h_r}{d}\frac{1}{c}B\right)\right|}{1+g(d)^2} \ . \tag{23}$$

Note that we are not able to derive the K-factor from the two-ray model. The two-ray model assumes a LOS component and one specular reflection, without modeling other, smaller components, thus $\sigma \to 0$ and hence $K \to \infty$. In Fig. 4 we compare the obtained parameter fits with the predicted values of our proposed model (black dashed lines). The ML fitted K-factor shows a negative trend with increasing distance. Remember that we employ directive antennas that illuminate a bigger area at larger distances and hence allow reflections from more and more surrounding buildings. The predicted Δ-parameters from (23) agree well with the ML estimated parameters.

IV. Conclusion

We have shown that both the two-ray model and the TWDP model can be easily parametrized by geometry, bandwidth and antenna directivity to accurately reproduce ray-tracing data. Both models can be directly applied in link-level simulations to study effects on the physical layer. Furthermore, since we have found closed-form solutions for the mean SNR as well as for the SNR fluctuations, a simplified base station placement and antenna tilting analysis is possible even without running simulations.

References

[1] H. Meinel and A. Plattner, "Millimetre-wave propagation along railway lines," in *IEE Proceedings F (Communications, Radar and Signal Processing)*, vol. 130, no. 7. IET, 1983, pp. 688–694.

[2] A. Kato, K. Sato, M. Fujise, and S. Kawakami, "Propagation characteristics of 60-GHz millimeter waves for ITS inter-vehicle communications," *IEICE Transactions on Communications*, vol. 84, no. 9, pp. 2530–2539, 2001.

[3] V. Va, T. Shimizu, G. Bansal, and R. W. Heath Jr, "Millimeter wave vehicular communications: A survey," *Foundations and Trends® in Networking*, vol. 10, no. 1, pp. 1–113, 2016.

[4] B. Ai, X. Cheng, T. Kürner, Z.-D. Zhong, K. Guan, R.-S. He, L. Xiong, D. W. Matolak, D. G. Michelson, and C. Briso-Rodriguez, "Challenges toward wireless communications for high-speed railway," *IEEE Transactions on Intelligent Transportation Systems*, vol. 15, no. 5, pp. 2143–2158, 2014.

[5] B. Ai, K. Guan, M. Rupp, T. Kürner, X. Cheng, X.-F. Yin, Q. Wang, G.-Y. Ma, Y. Li, L. Xiong *et al.*, "Future railway services-oriented mobile communications network," *IEEE Communications Magazine*, vol. 53, no. 10, pp. 78–85, 2015.

[6] S. Caban, J. Rodas, and J. A. García-Naya, "A methodology for repeatable, off-line, closed-loop wireless communication system measurements at very high velocities of up to 560 km/h," in *Proc. of IEEE Instrumentation and Measurement Technology Conference (I2MTC)*, 2011.

[7] L. Liu, C. Tao, T. Zhou, Y. Zhao, X. Yin, and H. Chen, "A highly efficient channel sounding method based on cellular communications for high-speed railway scenarios," *EURASIP Journal on Wireless Communications and Networking*, vol. 2012, no. 1, p. 307, 2012.

[8] J. Rodríguez-Piñeiro, P. Suárez-Casal, M. Lerch, S. Caban, J. A. Garcia-Naya, L. Castedo, and M. Rupp, "LTE downlink performance in high speed trains," in *Proc. of IEEE 81st Vehicular Technology Conference (VTC Spring)*, 2015.

[9] J. Rodríguez-Piñeiro, M. Lerch, J. A. García-Naya, S. Caban, M. Rupp, and L. Castedo, "Emulating extreme velocities of mobile LTE receivers in the downlink," *EURASIP Journal on Wireless Communications and Networking*, vol. 2015, no. 1, p. 106, 2015.

[10] C.-X. Wang, A. Ghazal, B. Ai, Y. Liu, and P. Fan, "Channel measurements and models for high-speed train communication systems: A survey." *IEEE Communications Surveys and Tutorials*, vol. 18, no. 2, pp. 974–987, 2016.

[11] E. Zöchmann, S. Schwarz, S. Pratschner, L. Nagel, M. Lerch, and M. Rupp, "Exploring the physical layer frontiers of cellular uplink," *EURASIP Journal on Wireless Communications and Networking*, vol. 2016, no. 1, p. 118, 2016.

[12] R. Nissel, E. Zöchmann, M. Lerch, S. Caban, and M. Rupp, "Low latency MISO FBMC-OQAM: It works for millimeter waves!" in *Proc. of IEEE International Microwave Symposium (IMS)*, 2017.

[13] R. Nissel, M. Rupp, and R. Marsalek, "FBMC-OQAM in doubly-selective channels: A new perspective on MMSE equalization," in *IEEE 18th International Workshop on Signal Processing Advances in Wireless Communications (SPAWC)*. IEEE, 2017, pp. 1–5.

[14] M. Saideh, M. Berbineau, and I. Dayoub, "On doubly selective channel estimation for FBMC-OQAM using the LMMSE filter for future railway communications," in *Proc. of 16th International Conference on Intelligent Transport Systems Telecommunications (ITST)*, 2018, pp. 1–6.

[15] E. Zöchmann, K. Guan, and M. Rupp, "Two-ray models in mmWave communications," in *Proc. of IEEE 18th International Workshop on Signal Processing Advances in Wireless Communications (SPAWC)*, 2017, pp. 1–5.

[16] H. Xia, H. L. Bertoni, L. R. Maciel, A. Lindsay-Stewart, and R. Rowe, "Radio propagation characteristics for line-of-sight microcellular and personal communications," *IEEE Transactions on Antennas and Propagation*, vol. 41, no. 10, pp. 1439–1447, 1993.

[17] M. J. Feuerstein, K. L. Blackard, T. S. Rappaport, S. Y. Seidel, and H. H. Xia, "Path loss, delay spread, and outage models as functions of antenna height for microcellular system design," *IEEE Transactions on Vehicular Technology*, vol. 43, no. 3, pp. 487–498, 1994.

[18] J. Kunisch and J. Pamp, "Wideband car-to-car radio channel measurements and model at 5.9 GHz," in *Proc. of IEEE Vehicular Technology Conference (VTC-Fall)*, 2008, pp. 1–5.

[19] J. Karedal, N. Czink, A. Paier, F. Tufvesson, and A. F. Molisch, "Path loss modeling for vehicle-to-vehicle communications," *IEEE Transactions on Vehicular Technology*, vol. 60, no. 1, pp. 323–328, 2011.

[20] C. Sommer, S. Joerer, and F. Dressler, "On the applicability of two-ray path loss models for vehicular network simulation," in *Proc. of IEEE Vehicular Networking Conference (VNC)*, 2012, pp. 64–69.

[21] E. Zöchmann, M. Lerch, S. Caban, R. Langwieser, C. F. Mecklenbräuker, and M. Rupp, "Directional evaluation of receive power, Rician K-factor and RMS delay spread obtained from power measurements of 60 GHz indoor channels," in *Proc. of IEEE-APS Topical Conference on Antennas and Propagation in Wireless Communications (APWC)*, Cairns, Australia, Sep. 2016.

[22] E. Zöchmann, M. Lerch, S. Pratschner, R. Nissel, S. Caban, and M. Rupp, "Associating spatial information to directional millimeter wave channel measurements," in *Proc. of IEEE Vehicular Technology Conference (VTC-Fall)*, 2017, pp. 1–5.

[23] N. Iqbal, D. Dupleich, C. Schneider, J. Luo, R. Müller, S. Hafner, G. Del Galdo, and R. S. Thomä, "Modeling of intra-cluster multipaths for 60 GHz fading channels," in *Proc. of IEEE European Conference on Antennas and Propagation (EuCAP)*, 2018.

[24] T. Blazek, E. Zöchmann, and C. F. Mecklenbräuker, "Approximating clustered millimeter wave vehicular channels by sparse subband fitting," in *Proc. of IEEE 29th Annual International Symposium on Personal, Indoor and Mobile Radio Communications (PIMRC)*, 2018, pp. 91–95.

[25] J. Blumenstein *et al.*, "Measured high-resolution power-delay profiles of nonstationary vehicular millimeter wave channels," in *Proc. of IEEE 29th Annual International Symposium on Personal, Indoor and Mobile Radio Communications (PIMRC)*, 2018, pp. 1–5.

[26] E. Zöchmann, C. F. Mecklenbräuker, M. Lerch, S. Pratschner, M. Hofer, D. Löschenbrand, J. Blumenstein, S. Sangodoyin, G. Artner, S. Caban, T. Zemen, A. Prokes, M. Rupp, and A. F. Molisch, "Measured delay and Doppler profiles of overtaking vehicles at 60 GHz," in *Proc. of the 12th European Conference on Antennas and Propagation (EuCAP)*, 2018, pp. 1–5.

[27] T. Blazek, E. Zöchmann, and C. F. Mecklenbräuker, "Model order selection for LASSO fitted millimeter wave vehicular channel data," in *Proc. of IEEE 29th Annual International Symposium on Personal, Indoor and Mobile Radio Communications (PIMRC)*, 2018, pp. 80–84.

[28] N. Iqbal, J. Luo, D. Dupleich, S. Häfner, R. Müller, C. Schneider, and R. S. Thomä, "Second-order statistical characterization of the 60 GHz cluster fading channels," in *Proc. of IEEE 29th Annual International Symposium on Personal, Indoor and Mobile Radio Communications (PIMRC)*, 2018, pp. 241–245.

[29] T. Blazek, E. Zöchmann, and C. Mecklenbräuker, "Millimeter wave vehicular channel emulation: A framework for balancing complexity and accuracy," *Sensors*, vol. 18, no. 11, p. 3997, 2018.

[30] E. Zöchmann, S. Caban, C. F. Mecklenbräuker, S. Pratschner, M. Lerch, S. Schwarz, and M. Rupp, "Better than Rician: modelling millimetre wave channels as two-wave with diffuse power," *EURASIP Journal on Wireless Communications and Networking*, vol. 2019, no. 1, pp. 1–21, 2019.

[31] A. Yamamoto, K. Ogawa, T. Horimatsu, K. Sato, and M. Fujise, "Effect of road undulation on the propagation characteristics of inter-vehicle communications in the 60 GHz band," in *Proc. of IEEE/ACES International Conference on Wireless Communications and Applied Computational Electromagnetics*, 2005, pp. 841–844.

[32] K. Guan, G. Li, T. Kürner, A. F. Molisch, B. Peng, R. He, B. Hui, J. Kim, and Z. Zhong, "On millimeter wave and THz mobile radio channel for smart rail mobility," *IEEE Transactions on Vehicular Technology*, vol. PP, no. 99, pp. 1–1, 2016.

[33] J. Frolik, "A case for considering hyper-Rayleigh fading channels," *IEEE Transactions on Wireless Communications*, vol. 6, no. 4, 2007.

[34] ——, "On appropriate models for characterizing hyper-Rayleigh fading," *IEEE Transactions on Wireless Communications*, vol. 7, no. 12, 2008.

[35] D. W. Matolak and J. Frolik, "Worse-than-Rayleigh fading: Experimental results and theoretical models," *IEEE Communications Magazine*, vol. 49, no. 4, 2011.

[36] M. Peter, W. Keusgen, and R. J. Weiler, "On path loss measurement and modeling for millimeter-wave 5G," in *Proc. of IEEE European Conference on Antennas and Propagation (EuCAP)*, 2015, pp. 1–5.

[37] R. Vaughan and J. Andersen Bach, *Channels, propagation and antennas for mobile communications*. IET, 2003.

[38] S. Priebe, M. Jacob, and T. Kürner, "The impact of antenna directivities on THz indoor channel characteristics," in *Proc. of 6th European Conference on Antennas and Propagation (EUCAP)*, 2012.

[39] G. D. Durgin, T. S. Rappaport, and D. A. De Wolf, "New analytical models and probability density functions for fading in wireless communications," *IEEE Transactions on Communications*, vol. 50, no. 6, pp. 1005–1015, 2002.

[40] M. Rao, F. J. Lopez-Martinez, M.-S. Alouini, and A. Goldsmith, "MGF approach to the analysis of generalized two-ray fading models," *IEEE Transactions on Wireless Communications*, vol. 14, no. 5, pp. 2548–2561, 2015.

[41] E. Zöchmann, M. Hofer, M. Lerch, S. Pratschner, L. Bernadó, J. Blumenstein, S. Caban, S. Sangodoyin, H. Groll, T. Zemen, A. Prokeš, M. Rupp, A. F. Molisch, and C. F. Mecklenbräuker, "Position-specific statistics of 60 GHz vehicular channels during overtaking," *IEEE Access*, pp. 1–1, 2019.